Evolution of mechanical and hydraulic properties in sandstone induced by simulated mineral trapping of CO2 geo-sequestration

AUTHOR(S):

Yasuhara, Hideaki; Kinoshita, Naoki; Lee, Dae Sung; Choi, Junhyung; Kishida, Kiyoshi

CITATION:

Yasuhara, Hideaki ...[et al]. Evolution of mechanical and hydraulic properties in sandstone induced by simulated mineral trapping of CO2 geo-sequestration. International Journal of Greenhouse Gas Control 2017, 56: 155-164

ISSUE DATE:

2017-01

URL:

http://hdl.handle.net/2433/219023

Evolution of mechanical and hydraulic properties in sandstone induced by simulated mineral trapping of CO_2 geo-sequestration

Hideaki Yasuhara[1*], Naoki Kinoshita[1], Dae-Sung Lee[2], Jun-Hyung Choi[2], and Kiyoshi Kishida[3]

[1] Department of Civil and Environmental Engineering, Ehime University, Matsuyama, 790-8577, JAPAN.

[2] Department of Energy and Mineral Resources Engineering, Dong-A University, Busan, KOREA.

[3] Department of Urban Management, Kyoto University, Kyoto, 615-8540, JAPAN.

*Corresponding Author, hide@cee.ehime-u.ac.jp; Tel&Fax: + 81-89-927-9853

Abstract

The CO_2 geo-sequestration has been studied as a countermeasure against global warming. When the injected CO_2 reacts with rock minerals, some portion may precipitate ultimately to carbonate minerals such as calcite and be trapped within the injected reservoir. It is of significant importance to examine how the mineral trapping exerts an influence on the mechanical, hydraulic, and transport properties in the targeted reservoir rocks because the trapped minerals may influence the integrity of the reservoir rocks, although such works are quite sparse in the literature. In this study, the influence of the mineral trapping on the evolution of the physical properties was evaluated by replicating the precipitation of calcite that may occur in the mineral trapping process. The calcite precipitation was enhanced artificially to occur within the void spaces of the Berea sandstone. Subsequently, the treated samples were examined by the mechanical and the permeability experiments. The experimental results revealed that approximately 10 % substitution of the void spaces by the precipitated calcite increased the modulus twofold and UCS by 20 %, and decreased the permeability by one order of magnitude, which should exert a favorable impact on the integrity of the reservoir against the leakage risks of the injected CO_2. A cementation theory revealed the serial process of the calcite precipitation occurring on the free-surface of grains and at the grain contacts. The predictions of the permeability using the Kozeny-Carman equation clarified the increase of the surface roughness of

grains with the increase of the calcite precipitation.

Keywords: CO_2 geo-sequestration, Mineral trapping, Calcite, Physical properties

Key Points:

- **Mineral trapping was simulated by in-situ calcite precipitation.**
- **Mechanical properties were improved by the simulated mineral trapping.**
- **Permeability decreased with the increase of precipitation.**
- **Permeability was predicted using the Kozeny-Carman equation.**

1. Introduction

As is well known, the CO_2 geo-sequestration may be one of the solutions so as to mitigate the global warming. It is of significant importance to address coupled thermal-hydraulic-mechanical-chemical processes when considering the long-term underground isolation of anthropogenic CO_2. The CO_2-water-rock interactions should play an important role in assessing the CO_2 injectivity (Czernichowski-Lauriol et al., 1996; Fischer et al., 2013). As the injected CO_2 reacts with rock minerals, carbonate minerals such as calcite may precipitate as the secondary minerals, and occupy the pore spaces to some degree, which is called the mineral

47 trapping of CO_2 (Gunter et al., 1993; Bachu et al., 1994). Consequently, the mechanical and the
48 hydraulic properties of the rocks should evolve. Thus, it is essential to examine quantitatively how
49 such the mineral trapping exerts an influence on those properties. Due to the carbonate
50 precipitation, the permeability of the host rocks may decrease and limit the extent of mineral
51 reactions (Hövelmann et al., 2012), and the elasticity may be improved. The influence of the
52 mineral trapping exerted on the evolution of the mechanical and the hydraulic properties may be
53 significant. However, the direct observation of the mineral trapping is difficult because it is
54 believed to be comparatively slow, maybe taking thousand years or even longer (IPCC, 2005).
55 Therefore, the laboratory experiments focusing on the effect of the mineral trapping on those
56 properties are quite sparse. Tarkowski et al. (2015) have conducted the 20-month experiments on
57 brine-rock-CO_2 interactions to investigate the change of the petrophysical parameters due to the
58 mineral trapping, concluding that the property of the reservoir rocks did not change significantly.
59 However, the experimental period should be too short to fully understand the process of the
60 mineral trapping and they have not examined the changes of the mechanical and the hydraulic
61 properties.

62 To overcome the difficulty in directly observing the mineral trapping, the enhanced mineral
63 trapping technique was proposed by Naganuma et al. (2011). In the system, bacteria were used to
64 accelerate the carbonate precipitation, and the efficacy of the microbially induced carbonate

65 precipitation (MICP) was confirmed. Originally, the MICP has been applied in the geotechnical
66 engineering to improve the deformation and strength properties of soils (Whiffin et al., 2007;
67 Ivanov and Chu, 2008; Mitchell and Santamarina, 2005; DeJong et al., 2010; Harkes et al., 2010;
68 van Paassen, 2011), and in the concrete engineering to improve the strength and durability of
69 concrete and mortar (Qian et al., 2010; Achal et al., 2013). The research on the MICP has been
70 mainly conducted using ureolytic bacteria (e.g., *Sporosarcina pasteurii*). These bacteria produce
71 precipitated calcite by a urease enzyme. In this MICP technique, the transport and the fixation of
72 the bacteria of interest are significant issues for achieving a suitable level of improvement of the
73 saturated porous media, and thus, have been studied to this end (Murphy and Ginn 2000; Froppen
74 and Shijven 2006; Whiffin et al. 2007; Harkes et al. 2010). In this work, the urease enzyme was
75 adopted, instead of using bacteria, to accelerate the calcite precipitation, which was proposed by
76 Yasuhara et al., (2012). Utilizing the enzyme itself is more straightforward than using bacteria,
77 because the cultivation and fixation of bacteria (i.e., biological treatment) do not need to be
78 considered. Again, in the MICP the microbial metabolism is a key factor, and it may be
79 impossible to constrain the extinction and/or the generation of living bacteria in natural
80 environments. In contrast, the enzyme-mediated calcite precipitation (EMCP) (Yasuhara et al.,
81 2012; Neupane et al., 2013) can exclude the laborious biological treatments.

82 In this study, the evolution of the mechanical and the hydraulic properties in Berea sandstone

with initial porosity of ~0.23 was examined quantitatively by replicating the mineral trapping process. The artificially accelerated mineral trapping was achieved by injecting the grouting materials (i.e., the EMCP technique), resulting in a rapid calcite precipitation within the pore spaces. The amount of the precipitated calcite can be controlled by changing the concentrations of the materials and the total injection volume. The measurements of the P-wave velocity, uniaxial compressive experiments, and the permeability experiments were conducted to examine the changes of the elasticity (i.e., the P-wave velocity and the elastic modulus), the uniaxial compressive strength, and the permeability due to the calcite precipitation. Note that in the mineral trapping process, several secondary carbonate minerals such as calcite ($CaCO_3$), dolomite ($CaMg(CO_3)_2$), siderite ($FeCO_3$), and dawsonite ($NaAlCO_3(OH)_2$) may be precipitated (Xu et al., 2003), but the effect of calcite only was examined in this work.

2. Experimental methods

2.1. Rock samples and gout materials

In this study, totally 47 cylindrical samples, whose names are called BS-1 – BS-47, 30 mm in diameter and 60 mm in height were made of a block of Berea sandstone (**Fig. 1**). Note that all the samples were cored parallel to the bedding planes, meaning that the flow direction of the grout injections and that in the permeability experiments were also parallel to them. It makes the grout

injections easier than being perpendicular to the bedding planes because the cores parallel to them have higher permeability. Before the grout injections, the initial porosity of all the samples were measured and was found to be ~0.23. The representative chemical compositions were determined by X-ray fluorescence (XRF) (Yasuhara et al., 2015a). The weight percentages of the major elements are listed in **Table 1**. In addition, the mineral compositions, before the grout injections, were also determined by X-ray diffraction (XRD) (Yasuhara et al., 2015b) and are shown in **Fig.2**. Berea sandstone is composed almost completely of pure quartz, but also contains slight amounts of feldspars, dolomite, and kaolinite.

The grouting materials adopted in the EMCP technique are composed of urea, urease, and $CaCl_2$ (Yasuhara et al., 2012), and were injected in the samples to simulate the mineral trapping by the artificially-enhanced calcite precipitation. The urease, purified from the jack bean meal, having urease activity of 2950 U/g, has been used in the bio-catalytic dissociation of urea. The reactions to obtain the calcite precipitation, enhanced by the effect of urease, are expressed as follows,

$$CO(NH_2)_2 + 2H_2O \rightarrow 2NH_4^+ + CO_3^{2-} \quad (1)$$

$$CaCl_2 \rightarrow Ca^{2+} + 2Cl^- \quad (2)$$

$$Ca^{2+} + CO_3^{2-} \rightarrow CaCO_3 \downarrow \quad (3)$$

where $CO(NH_2)_2$ represents the urea. The urease was used to accelerate the reaction shown in Eq.

(1).

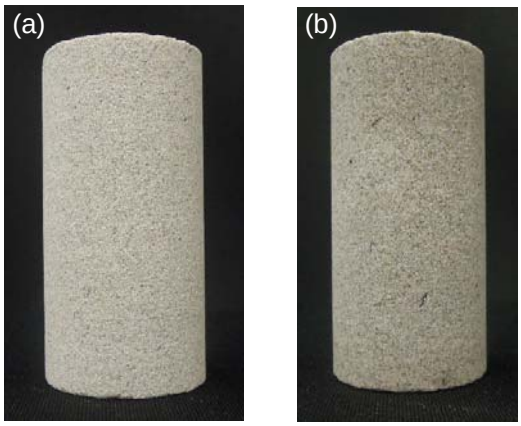

Fig. 1. Rock sample made of Berea sandstone ((a) before injection, (b) after injection).

Table 1. Composition of Berea sandstone (Yasuhara et al., 2015a).

Oxide	Results [wt.%]
SiO_2	82.6
Al_2O_3	9.88
Fe_2O_3	2.13
SO_3	-
K_2O	1.97
CaO	1.66
MgO	0.973
Na_2O	-
TiO_2	0.633
Cl	-
Others	0.154

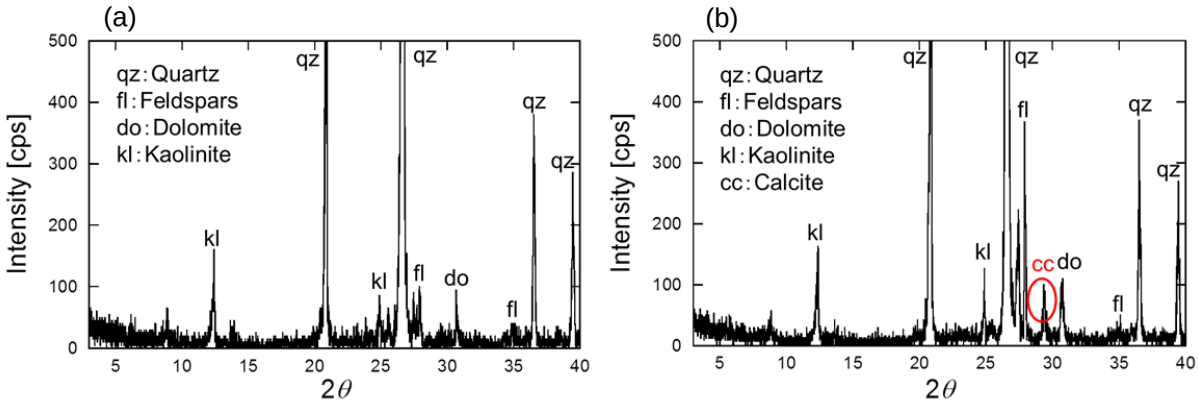

Fig. 2. Mineral composition of rock samples determined by XRD

((a) before injection, (b) after injection (BS-24)) (Yasuhara et al., 2015b).

2.2. *Procedure of calcite precipitation*

When simulating the mineral trapping by the calcite precipitation, uniform distribution of the precipitation within the rock samples should be achieved to quantitatively investigate the change of the mechanical and the hydraulic properties induced by the precipitation. To this end, an organized procedure for injecting the grout materials was developed. Using the experimental setup (**Fig. 3**) (Yasuhara et al., 2015b), the injections of the grout materials composed of urea, urease, and $CaCl_2$ were conducted by the following steps. Firstly, the rock samples were immersed in a beaker filled with de-ionized water and then placed inside a desiccator.

144 Subsequently, the space in the desiccator was evacuated by a vacuum pump for 24 hours in order
145 to remove air from the rock samples. After the saturation process, the rock sample was confined
146 within a heat-shrink tube. Once the core was jacketed, it was placed inside a pressure cell.
147 Subsequently, axial pressure was prescribed by disc springs and controlled well by a load cell
148 mounted onto the springs. Confining pressure, equivalent to the axial pressure, was applied by a
149 hand pump and controlled by a regulator. In this work, 3 MPa was applied as the axial and the
150 confining pressure to simulate the subsurface condition. Throughout the grout injections and the
151 following permeability experiments were conducted under the pressure. After the rock sample
152 was placed in the pressure cell, the concentration-adjusted grout materials were injected into the
153 sample. The amount of each injection was 10 mL, which is roughly equivalent to the whole pore
154 volume of each rock sample. Because the calcite precipitation starts within 30 minutes after the
155 injection (Yasuhara et al., 2012), each injection was complete within 15 minutes. Then, the
156 sample was placed quietly in the cell for 24 hours to wait for cease of the precipitation. After the
157 24-hour curing time, de-ionized water was injected to flush the byproduct of NH_4Cl that is
158 included in the grout materials (see Eqs. (1) and (2)). Note that it was confirmed that the
159 byproducts was completely flushed out by the water injection. Subsequently, the above process
160 was repeated as long as the grout injection could be complete within 15 minutes. Therefore, if the
161 injection was not complete within the time, the injected grout was quickly flushed by de-ionized

water to avoid non-uniform precipitation within the rock samples.

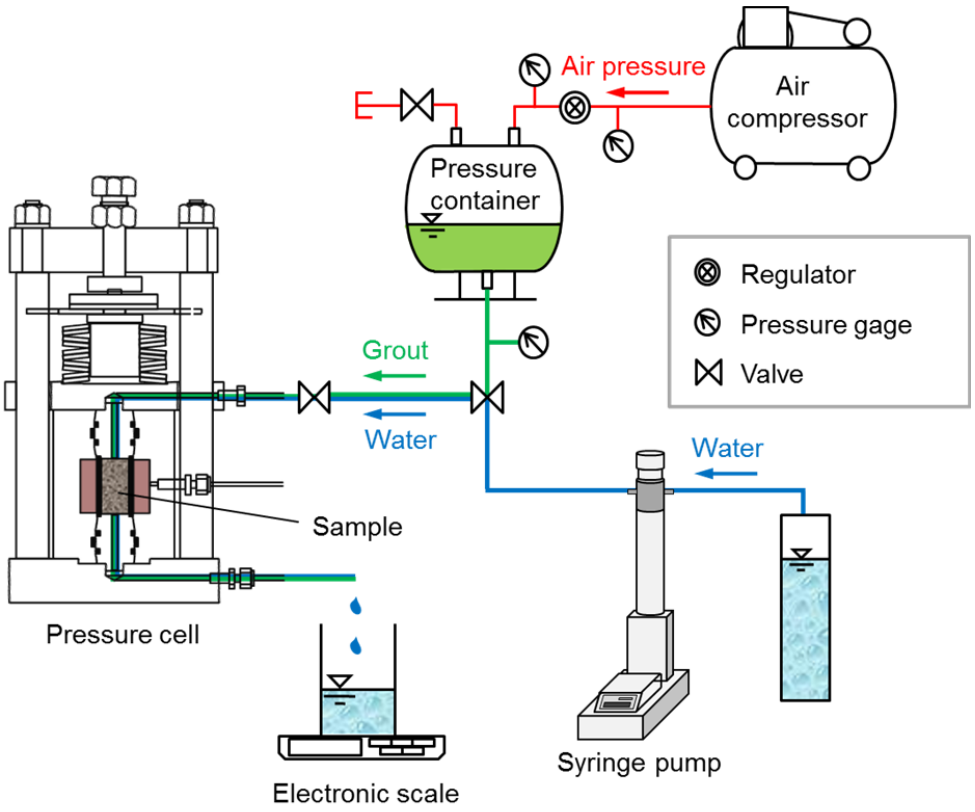

Fig. 3. Experimental setup for grout injections and permeability experiments (Yasuhara et al., 2015b).

2.3. *Petrographic and microstructural observations*

The mineralogical alteration in the samples before and after the grout injections were analyzed using XRD to identify the kinds of the precipitated minerals. The rock samples for the XRD analyses were ground to obtain the powder samples. The ground particles were rinsed by

methanol for several times to remove the dusts remaining on the surfaces. Then, the particle samples were observed by XRD to identify the minerals and to examine the difference between the samples before and after the grout injections.

The microstructures of the rock samples were analyzed by an optical microscope to investigate the size and shape of the precipitated minerals. The rock samples were prepared by making a single fracture induced by the Brazilian tests. Then, fresh fracture surfaces opened by the tests were analyzed by the microscope. Two samples, one before the grout injections and the other after the injections, were observed to compare the differences. The pore size distributions of the samples before and after the grout injections were also observed by mercury porosimetry. Because the distributions may change due to the precipitation, the analysis results may be congruent with the microscope observations.

Another concern arising from the grout injections is whether a uniform distribution of the precipitation within the rock samples could be achieved. It is important to obtain the uniformity to examine the evolution of the mechanical and the hydraulic properties in the treated samples. If secondary minerals induced by the grout injections precipitate quite locally within the samples (e.g., concentrating close to the injection inlet), the relation between the amount of the precipitation and those properties evaluated through the experiments would be unreliable. To check the distribution of the precipitated minerals, a treated sample was cored by a core drill and

then, the core was cut by a saw to three pieces (**Fig. 4**). By evaluating the amount of the precipitation for the treated sample before cored, the three inner cores, and the cored outer sample, the precipitation distribution within the sample can be clarified.

As an index of evaluating the amount of precipitation within the samples, the pore occupation ratio, R_p, was defined by,

$$R_p = \frac{V_c}{V_{v0}} \tag{4}$$

where V_c is the volume of the precipitated material (m^3), and V_{v0} is the initial pore volume of the sample before the grout injections (m^3). The pore volume, V_{v0}, can be obtained by calculating the porosity, given by,

$$\phi = \frac{\rho_g - \rho_d}{\rho_g} \tag{5}$$

$$V_{v0} = \phi \cdot V \tag{6}$$

where ϕ is the porosity of the sample (-), ρ_g is the grain density of the Berea sandstone (= 2700 kg m^{-3}), and ρ_d is the dry density of the samples (kg m^{-3}). The evolution of the mechanical and the hydraulic properties were examined using this index in this work.

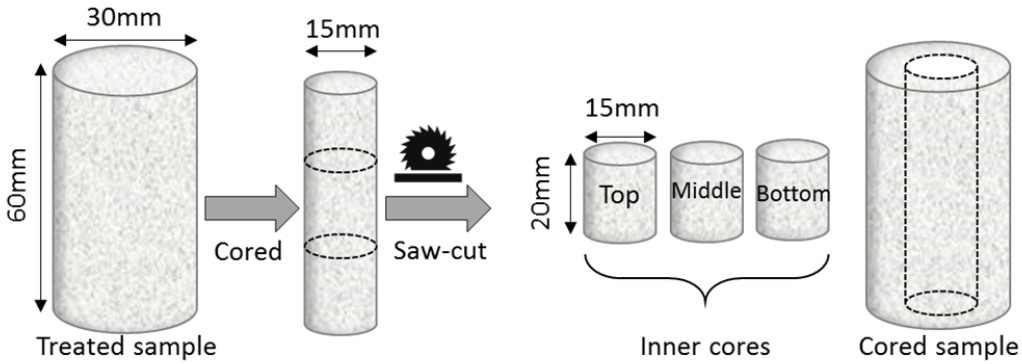

Fig. 4. Procedure to obtain the samples for examining the precipitation distribution.

2.4. Mechanical experiments

The P-wave velocity of the rock samples before and after the grout injections was measured by a device. Prior to each measurement, the samples were completely dried within an oven at 60 °C for 8 hours. The velocity was measured three times for each measurement to avoid the observation errors.

The uniaxial compression experiments were also conducted to obtain the elastic modulus and the uniaxial compression strength (UCS) of the rock samples before and after the grout injections. Two pieces of the two-axle strain gauges were pasted on the surface of the samples to measure the vertical and horizontal strains. Then, the samples were set onto the compression table and the displacement–controlled compression was statically conducted with the velocity of 0.10 mm s^{-1} until the failure. Subsequently, the UCS and the secant elastic modulus (E_{s50} in this work) were evaluated to examine the change of the mechanical properties induced by the mineral

precipitation.

2.5. *Permeability experiments*

Permeability experiments using the setup as shown in **Fig. 3**, were conducted to obtain the relation between the pore occupation ratio and the measured permeability. Those were performed after each grout injection with the differential water pressure of 100 kPa. The permeability was evaluated by assuming a Darcian flow, given by,

$$k = \frac{\mu Q L}{A \Delta P} \tag{7}$$

where k is the intrinsic permeability (m^2), μ is the dynamic viscosity (Pa s), Q is the flow rate (m^3 s^{-1}), L is the sample height (m), A is the cross-sectional area (m^2), and ΔP is the differential water pressure (Pa). The measured permeability was also normalized by the initial values to examine the change of permeability with the pore occupation ratio. The procedure of the whole experiments including the grout injections, P-wave velocity measurements, permeability experiments, and uniaxial compression experiments can be depicted in **Fig. 5**.

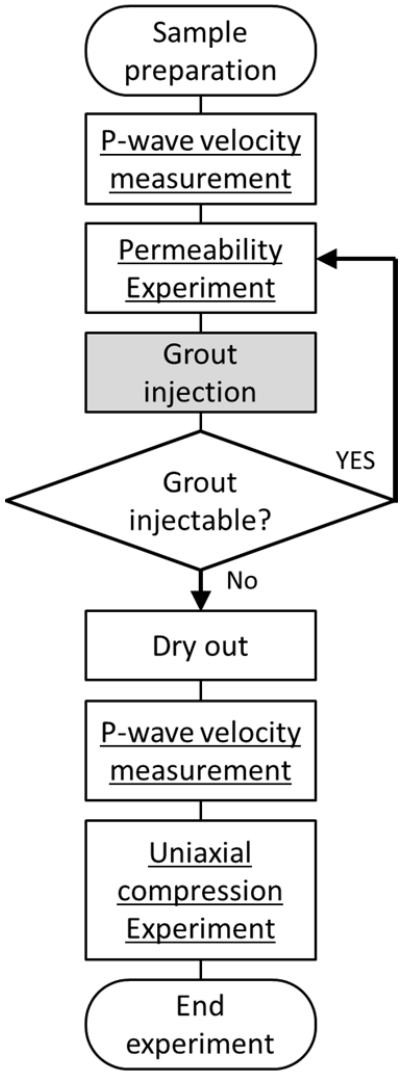

Fig. 5. Procedure of whole experiments including grout injections, P-wave velocity measurements, permeability experiments, and uniaxial compression experiments.

3. Experimental results

3.1. Confirmation of calcite precipitation

Prior to showing the results of the mechanical and the permeability experiments, the calcite

243 precipitation was confirmed by the XRD analysis and the optical microscope observations, which
244 was supplemented by the mercury porosimetry, and the distribution of the precipitated minerals
245 within the samples was evaluated by the method shown in section 2.3. The obtained XRD patterns
246 of the samples before and after the grout injections are shown in **Fig. 2**. As comparing the results
247 between the pre- and post-injection samples, a clear, unique peak of calcite is apparent in the
248 post-injection sample, and any other new peaks are not observed (**Fig. 2b**). Therefore, the
249 precipitated mineral induced by the grout injections was confirmed to be calcite only. The
250 photographs observed by the optical microscope are shown in **Fig. 6** (Yasuhara et al., 2015b). As
251 is clearly seen in **Fig. 6b**, the white particles smaller than the sand particles with a diameter of
252 approximately or more than 100 μm (**Fig. 6a**), lie onto the sand particles, and these should be
253 calcite. From this figure, the size of the calcite particles was found to range from several to a few
254 tens of microns.
255

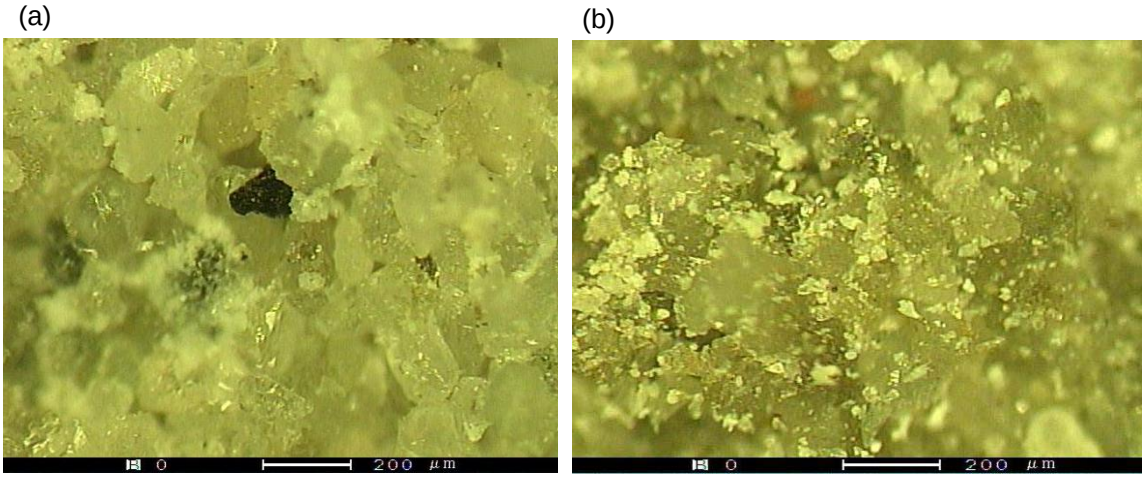

256

257 Fig. 6. Photographs of interior image of rock samples observed by optical microscope.

258 ((a) before injection, (b) after injection (BS-7)) (Yasuhara et al., 2015b).

259

260 The pore size distribution of the samples before and after the calcite precipitation was

261 analyzed by the mercury porosimetry (**Fig. 7**). Subtracting the frequency of the post-injection

262 measurements from that of the pre-injection results in the difference of relative frequency (**Fig.**

263 **7b**), clarifying how the pore radius distribution was changed by the calcite precipitation. Note that

264 the positive and negative values in **Fig. 7b** represent the increase and the decrease of the relative

265 frequency in the post-injection sample relative to the pre-injection, respectively. When comparing

266 the pore radii of the pre- and post-injection samples, the pores with a radius of less than 6 μm

267 increase and those with that of more than 6 μm decrease in the post-injection sample. This is

268 clearly attributed to the calcite precipitation. The results of the mercury porosimetry imply that the

269 diameter of the precipitated calcite is a few tens of microns, which is congruent with the

270 microscope observations.

271

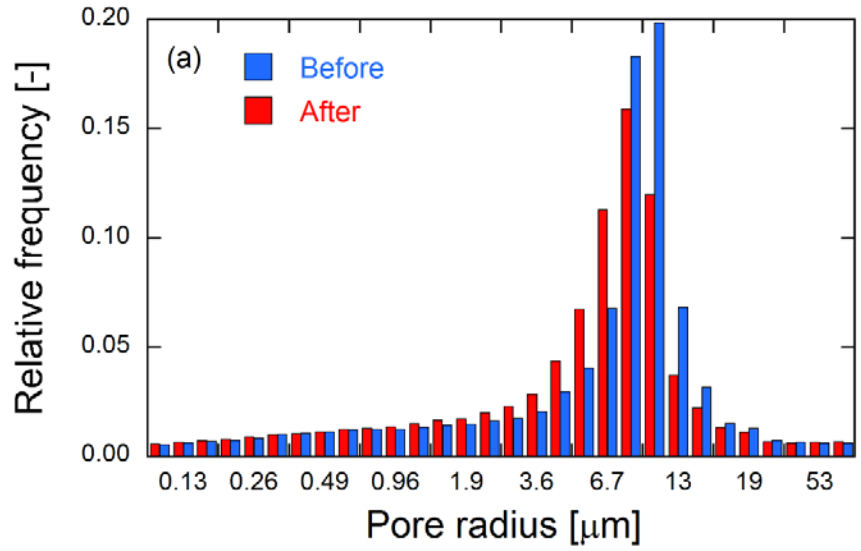

272

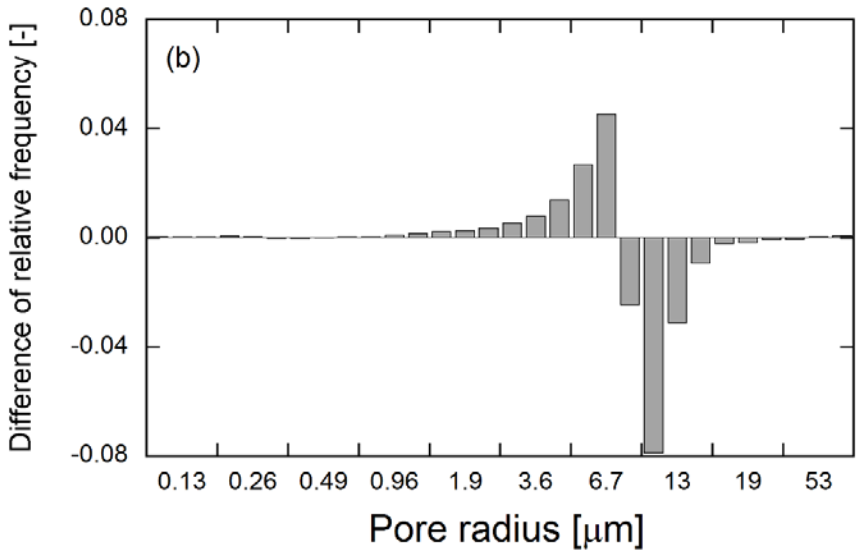

273

274 Fig. 7. Pore radius frequency in rock samples obtained by mercury porosimetry. The sample of

275 BS-36 was used for the porosimetry after the experiments. ((a) relative frequency of pore radius,

276 (b) difference of relative permeability).

277

278 The distribution of the calcite precipitation within the sample was evaluated by following the

279 procedure described in section 2.3 (see **Fig. 4**). The porosity, the pore occupation ratio, and
280 P-wave velocity were obtained for the three inner cores and the cored outer sample, supplemented
281 with the measurements for the whole core before cored (**Table 2**). The obtained porosity, pore
282 occupation ratio, and P-wave velocity are relatively compatible among all of the measured
283 samples, although the pore occupation ratio of the top core is slightly lower than the others.
284 Consequently, it can be judged that relatively uniform distribution of the calcite precipitation was
285 achieved and the grouting method adopted in this work was reliable.

286

287 Table 2. Measurements of pore occupation ratio and P-wave velocity (BS-44).

Sample		Porosity (-)	Pore occupation ratio (-)	P-wave velocity (km s^{-1})
Inner cores	Top	0.233	0.055	2.91
	Middle	0.227	0.071	3.08
	Bottom	0.238	0.072	2.94
Cored sample		0.179	0.079	-
Average values		0.227	0.075	2.97
Whole sample before cored		0.224	0.082	2.96

288

289 *3.2. Evolution in mechanical properties*

290 The P-wave velocity was measured for the pre- and post-injection samples. The measured
291 velocity for the post-injection samples was normalized by that measured before the injections (**Fig.**
292 **8a**). A linear relation between the pore occupation ratio (see Eq. (4)) and the normalized P-wave

velocity was clearly obtained. The obtained relation shows that the P-wave velocity increases by ~50 % when the pore occupation ratio reaches 0.10, which should exert a favorable influence on the integrity of the CO_2-injected reservoir against seismic motions. Using the measured P-wave velocity, the dynamic elastic modulus can be evaluated by (Jaeger et al., 2007),

$$E_D = \frac{V_p{}^2 \rho_d \left(1+\nu_D\right)\left(1-2\nu_D\right)}{1-\nu_D} \tag{8}$$

where E_D is the dynamic elastic modulus (Pa), V_p is the P-wave velocity (m s^{-1}), and ν_D is the dynamic Poisson's ratio (-). As the S-wave velocity was not measured in this work, not only the dynamic Poisson's ratio but also the dynamic elastic modulus cannot be directly evaluated. However, the change of the modulus, which is the evolved modulus normalized by the initial modulus of the pre-injection samples, may be able to be estimated by assuming the dynamic Poisson's ratio and the dry density to be constant throughout the calcite precipitation, which can be expressed as,

$$\frac{E_D}{E_{D0}} = \left(\frac{V_p}{V_{p0}}\right)^2 \tag{9}$$

where E_{D0} is the initial dynamic elastic modulus (Pa) and V_{p0} is the initial P-wave velocity (m s^{-1}) before the calcite precipitation. The normalized dynamic elastic modulus evaluated by Eq. (9) is shown in **Fig. 8b**. Similar to the measurements of the P-wave velocity (**Fig. 8a**), it linearly increases with the increase of the pore occupation ratio and augments twofold when the pore

310 occupation ratio reaches 0.10.

311

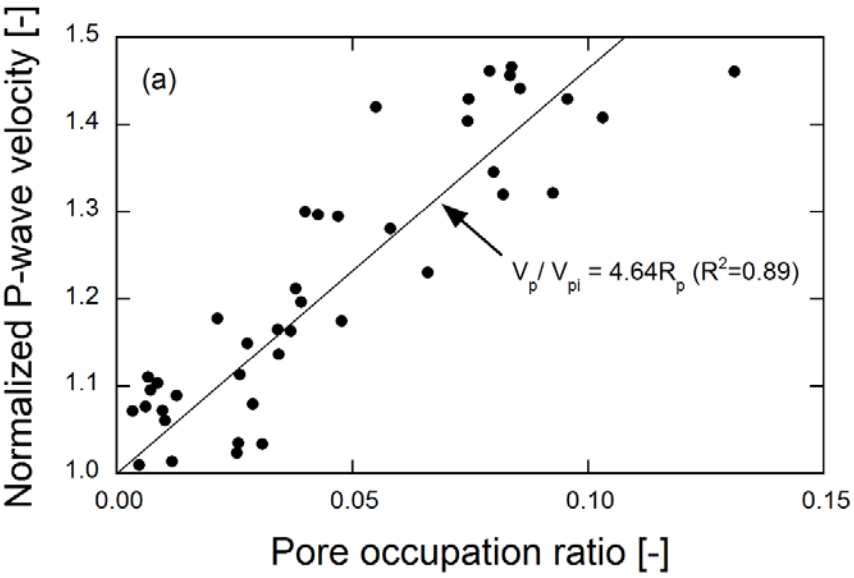

312

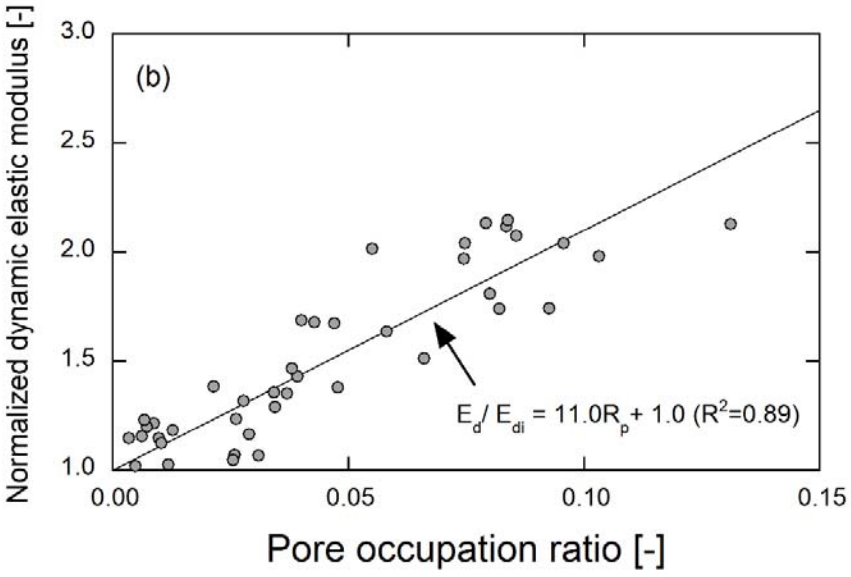

313

314 Fig. 8. Relation between pore occupation ratio and (a) normalized P-wave velocity and (b)

315 normalized dynamic elastic modulus.

316

317 The uniaxial compression experiments were also conducted to examine the change of the
318 mechanical properties induced by the calcite precipitation. The results of the experiments
319 elucidate the evolution of the static elastic modulus and the UCS (**Fig. 9**). Both of the elastic
320 modulus, E_{s50}, and the UCS increase linearly with the increase of the pore occupation ratio, and
321 augment twofold and by 20 % when it attains 0.10, respectively. Note that the increasing rates of
322 the dynamic and static elastic modulus (i.e., E_D and E_{s50}) coincide (see **Figs. 8b** and **9a**), and it
323 can be thought that our measurements are reliable. The mechanical experiments revealed that
324 clogging only the fraction of the pore spaces by the calcite precipitation significantly improves the
325 deformation/strength characteristics.

326

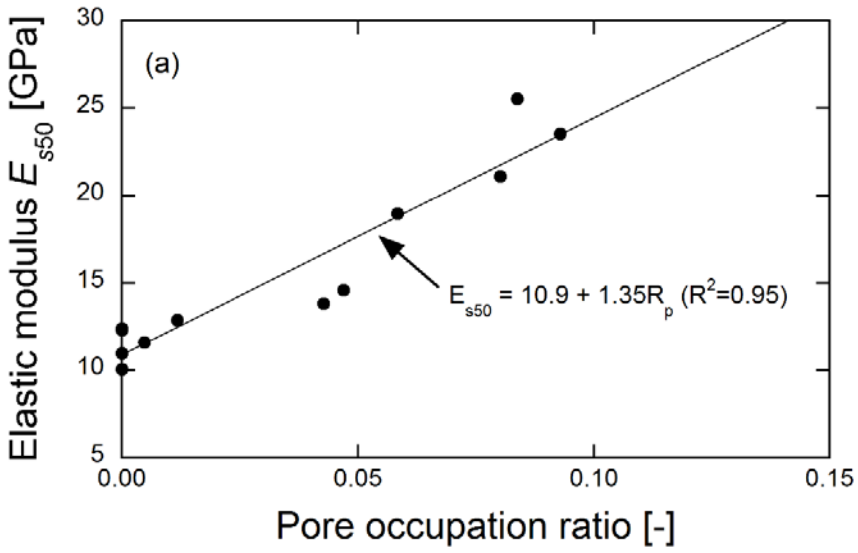

327

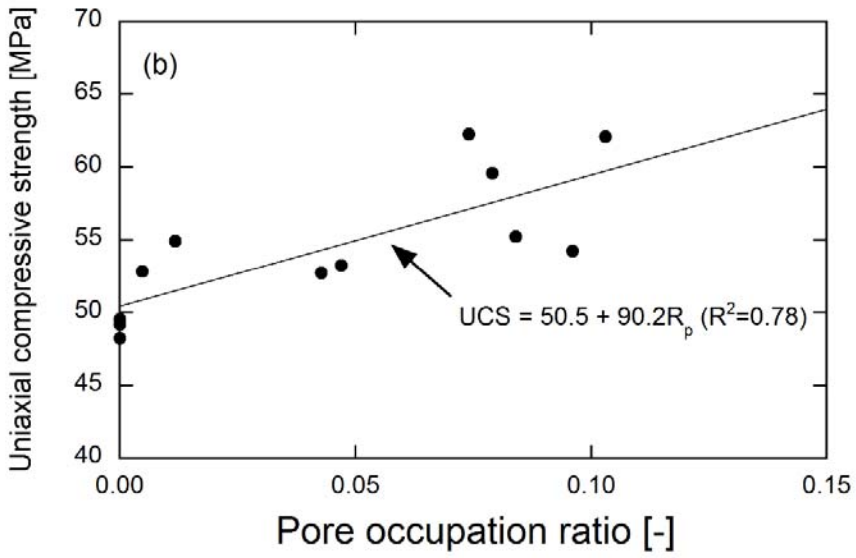

328

329 Fig. 9. Relation between pore occupation ratio and (a) elastic modulus, E_{s50}, and (b) UCS.

330

331 *3.3. Evolution in permeability*

332 The permeability experiments were conducted to examine the change of the permeability
333 induced by the calcite precipitation. The obtained permeability shows a decrease tendency with
334 the increase of the pore occupation ratio (**Fig. 10a**), but the tendency is ambiguous because of the
335 scattered data. Therefore, the measured permeability was initialized by the initial permeability
336 obtained before the grout injections (**Fig. 10b**). The normalization process made the decrease
337 tendency much clearer. The normalized permeability monotonically decreases with the increase of
338 the pore occupation ratio. Specifically, an abrupt decrease is observed after roughly 7 % - the
339 permeability at the occupation ratio of 9 % decrease by one order of magnitude. The reduction is

340 due to narrowing or clogging of the flow path by the calcite precipitation, which should also be
341 favorable to the confinement of the injected CO_2 in reservoirs.
342

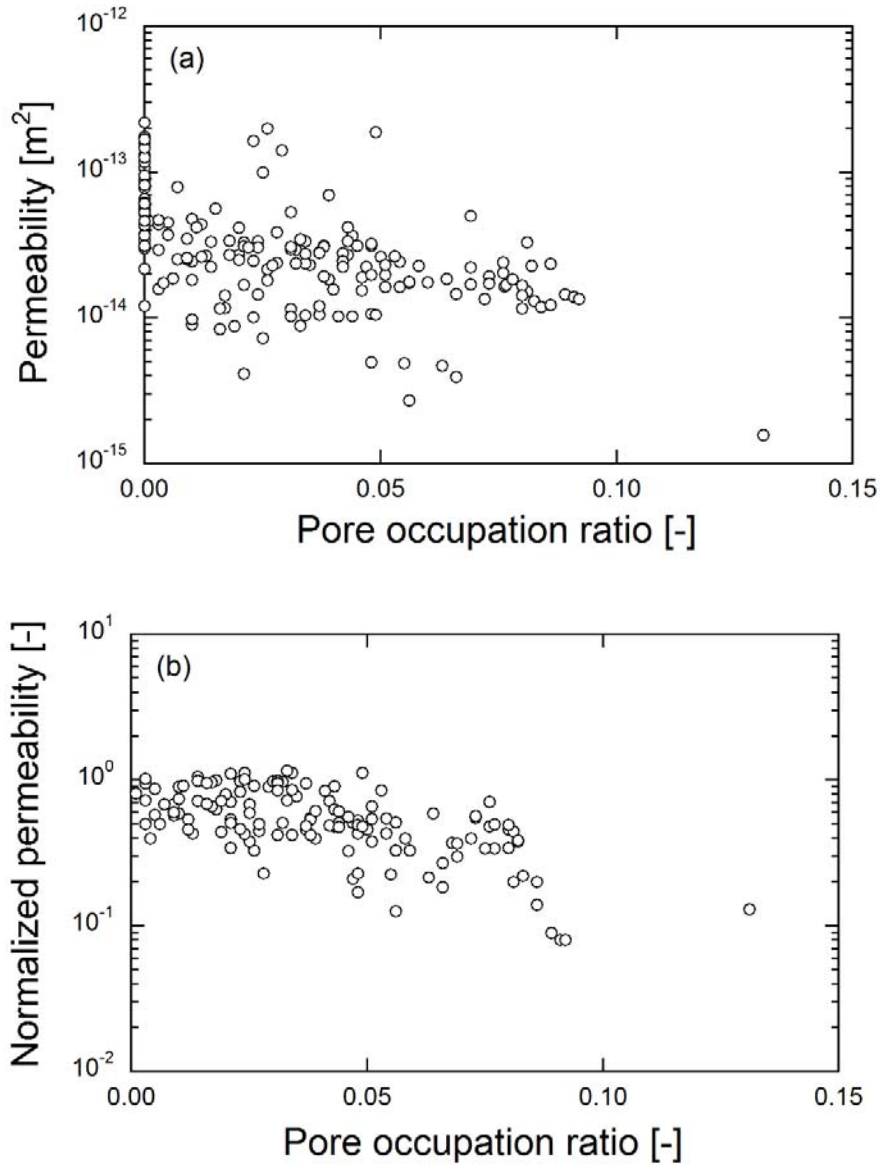

343
344

345 Fig. 10. Relation between pore occupation ratio and (a) permeability and (b) normalized
346 permeability.

4. Discussion

We have observed interesting results in the evolution of the mechanical and the hydraulic properties induced by the simulated mineral trapping (i.e., calcite precipitation) – the observed elastic modulus and the UCS increased with the increase of the calcite precipitation, while the permeability decreased with that. Firstly, to investigate the mechanisms of the change in elasticity, the P-wave velocity was estimated by following Dvorkin and Nur (1996). They model the P-wave velocity using a cementation theory where the grains mechanically interact through cement at the grain boundaries, given by,

$$V_p = \sqrt{\frac{6K_{eff}}{n(1-\phi_0)\rho_c S_n}} \tag{10}$$

where K_{eff} is the effective bulk modulus (Pa), n is the average number of contacts per grain (n = 9 (Dvorkin and Nur (1996))), ρ_c is the density of the cement material, which is calcite in this work (= 2710 kg m^{-3}), and S_n is the fitting parameter (-). S_n is expressed as (Dvorkin and Nur (1996)),

$$S_n = A_n(\Lambda_n)\alpha^2 + B_n(\Lambda_n)\alpha + C_n(\Lambda_n) \tag{11}$$

$$A_n(\Lambda_n) = -0.024153 \cdot \Lambda_n^{-1.3646} \tag{12}$$

$$B_n(\Lambda_n) = 0.20405 \cdot \Lambda_n^{-0.89008} \tag{13}$$

$$C_n(\Lambda_n) = 0.00024649 \cdot \Lambda_n^{-1.9846} \tag{14}$$

$$\Lambda_n = \frac{2G_c}{\pi G}\frac{(1-\nu)(1-\nu_c)}{1-2\nu} \tag{15}$$

where α is the ratio of the radius of the cement layer to the grain radius (-), G (Pa) and ν (-) are the shear modulus and the Poisson's ratio of the grains, respectively, and G_c (Pa) and ν_c (-) are the shear modulus and the Poisson's ratio of the contact cement layer, respectively. By assuming that porosity reduction is caused only by cementation (i.e., calcite precipitation) and by adopting certain schemes of cement deposition (Dvorkin and Nur (1996)), the ratio, α, can be related to the porosity amended by the calcite precipitation, as,

$$\alpha = 2\left[\frac{\phi_0 - \phi}{3n(1-\phi_0)}\right]^{0.25} \quad (\text{Scheme 1}) \tag{16}$$

$$\alpha = \left[\frac{2(\phi_0 - \phi)}{3(1-\phi_0)}\right]^{0.5} \quad (\text{Scheme 2}) \tag{17}$$

where Schemes 1 and 2 are defined as the cases where all cement is deposited at grain contacts and where cement is deposited evenly on the grain surface (**Fig. 11**). All the parameter values used to estimate the P-wave velocity are summarized in **Table 3**. The model predictions of the relation between the porosity and the P-wave velocity obtained by assuming the Scheme 1 or 2 are shown together with the experimental measurements (**Fig. 12a**), and those of the relation between the pore occupation ratio and the P-wave velocity are depicted in **Fig. 12b**. Note that the pore occupation ratio can be evaluated directly by the porosity, as,

$$R_p = 1 - \frac{\phi}{\phi_0} \tag{18}$$

As is apparent, the measurements are followed by the model of the Scheme 2 in the early stage at smaller calcite precipitation, and subsequently, those are followed by the Scheme 1. Therefore, the pore occupation process is thought to be that the calcite precipitation firstly occurs on the free-surface of the grains and that on the grain contacts dominate over the free-surface precipitation.

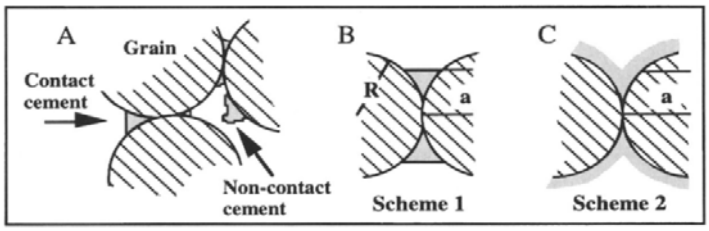

Fig. 11. Cemented grains ((a) Contact and noncontact cement, (b) Scheme 1 of cement deposition, and (c) Scheme 2 of cement deposition) (Dvorkin and Nur, 1996).

Table 3. Parameters in Eqs. (10)-(17) used to predict P-wave velocity.

K_{eff} (GPa)	n (-)	ϕ_0 (-)	ρ_c (kg m^{-3})	G (GPa)	G_c (GPa)	ν (-)	ν_c (-)
11.9	9	0.235	2710	44.0	14.0	0.22	0.32

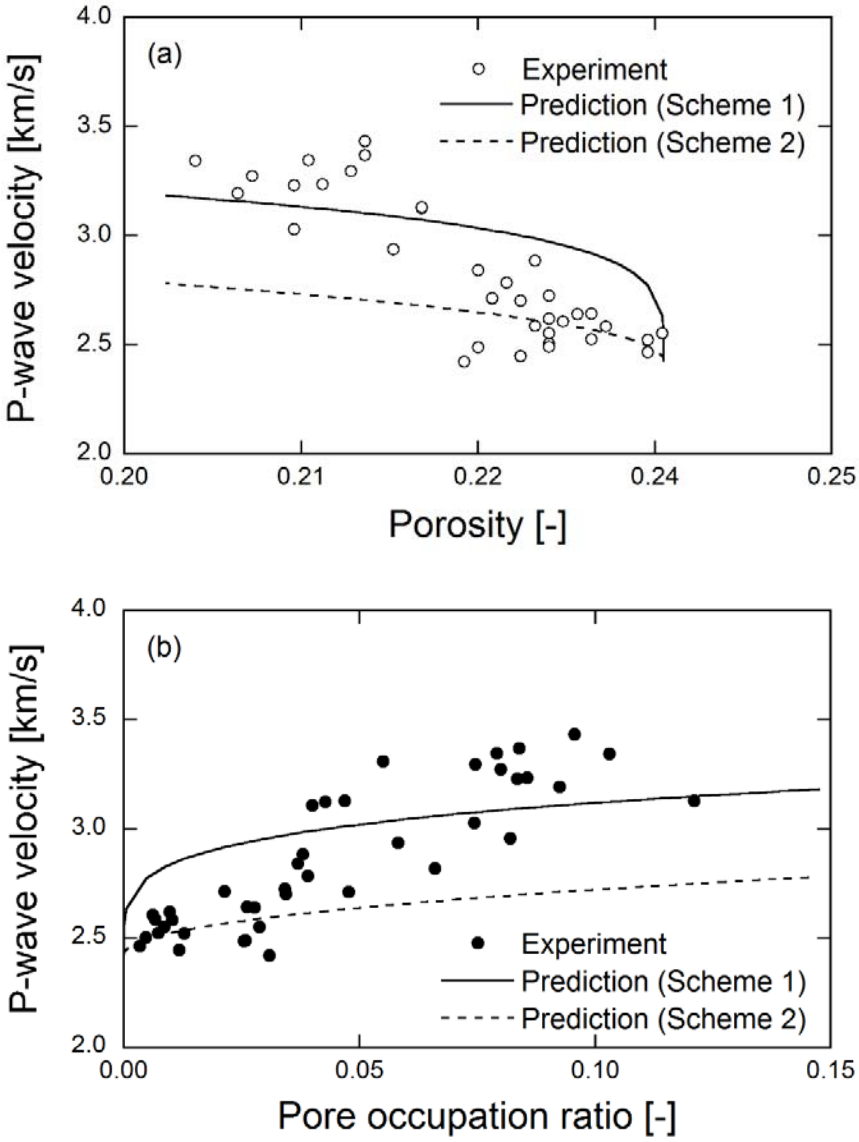

393

394

395 Fig. 12. Comparison between measurements and predictions of relation between P-wave velocity

396 and (a) porosity and (b) pore occupation ratio.

397

398 Secondly, to examine the mechanisms of the change in permeability, the experimental

399 measurements were predicted by the Kozeny-Carman equation (Bear, 1972), as,

$$k = \frac{1}{5S_v^2}\frac{\phi^3}{(1-\phi)^2} \tag{19}$$

where S_v is the specific surface are (m^2 m^{-3}). Eq. (19) can be rearranged with respect to the pore occupation ratio using Eq. (18), as,

$$k = \frac{1}{5S_v^2}\frac{\phi_0^3\left(1-R_p\right)^3}{\left(1-\phi_0\left(1-R_p\right)\right)^2} \tag{20}$$

Therefore, the permeability normalized by the initial permeability can be obtained as,

$$\frac{k}{k_0} = \left(\frac{S_{v0}}{S_v}\right)^2 \frac{\left(1-R_p\right)^3\left(1-\phi_0\right)^2}{\left(1-\phi_0\left(1-R_p\right)\right)^2} \tag{21}$$

where k_0 is the initial permeability (m^2), and S_{v0} is the initial specific surface area (m^2 m^{-3}). When the calcite precipitation occurs on the free-surface and/or the contacts of grains, the specific surface area should be changed. However, because it is clearly difficult to predict the change through the precipitation, a simple relation, defined as $S_v = S_{v0}\left(1+a\cdot R_p\right)$, is assumed to follow the measured permeability, and Eq. (21) can be rearranged as,

$$\frac{k}{k_0} = \left(\frac{1}{\left(1+a\cdot R_p\right)}\right)^2 \frac{\left(1-R_p\right)^3\left(1-\phi_0\right)^2}{\left(1-\phi_0\left(1-R_p\right)\right)^2} \tag{22}$$

where a is the constant (-). When the parameter a is zero, the specific surface area never changes from its initial value even if the calcite precipitation occurs. In contrast, when it is the positive or negative value, the specific surface area increases or decreases with the increase of the pore occupation ratio, respectively. As the calcite precipitation proceeds, the grain surface should be

416 rougher, which is supported by **Fig. 6**, and the specific surface area should increase accordingly.
417 Thus, the predictions with the positive values of *a* may result in better agreement with the
418 measurements. Actually, the experimental measurements are in disagreement with the prediction
419 as $a = 0$, while those are well-followed by the predictions with the positive values ranging from 5
420 to 20 (**Fig. 13**). This indicates that the specific surface area may increase by 1.5 – 3 times as the
421 pore occupation ratio reaches 0.10. Therefore, to achieve reliable predictions of the permeability
422 change induced by the mineral trapping (i.e., carbonate precipitation), the change of the specific
423 surface area should also be estimated with a certain level of precision in advance.
424

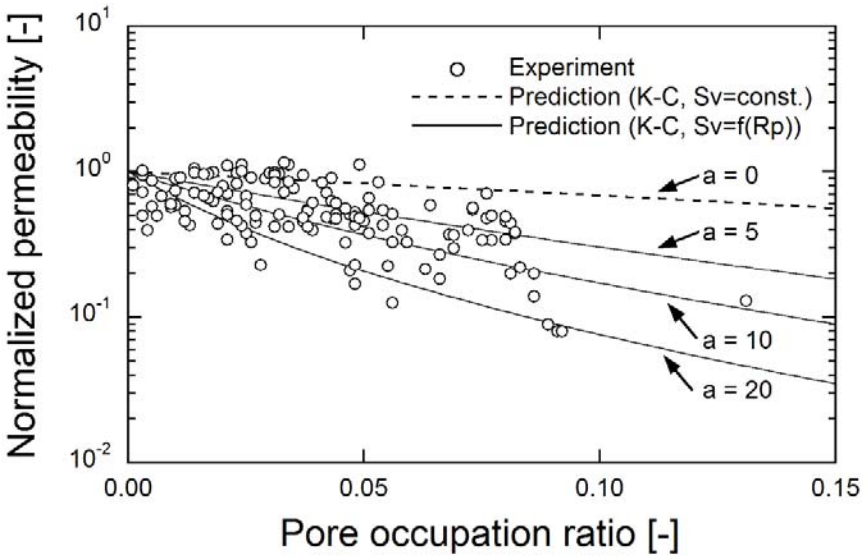

425
426 Fig. 13. Comparison of relation between pore occupation ratio and normalized permeability
427 between measurements and predictions.

5. Conclusions

In this work, the evolution of the mechanical and the hydraulic properties were quantitatively examined by simulating the mineral trapping, which was achieved by the artificially-enhanced calcite precipitation using the EMCP technique. Before examining the change of those properties, uniform distribution of the calcite precipitation within the rock samples was confirmed by the XRD analyses, the optical microscope observations, the mercury porosimetry, and the direct measurements of the calcite amount.

Both of the estimated, normalized dynamic elastic modulus and the measured, static elastic modulus, and the UCS increased twofold and by ~20 % as the pore occupation ratio attained 0.10, respectively. The normalized permeability decreased by one order of magnitude at it reached 0.10. From the measurements of the mechanical and the permeability experiments, we understood that occupying the fraction of the pore spaces dramatically exerts favorable influences on the integrity of the CO_2-injected reservoir.

A cementation theory proposed by Dvorkin and Nur (1996) enabled us to understand where the calcite selectively precipitated within the domain – firstly, the precipitation may have occurred evenly on the grain surface, and gradually it concentrated at grain contacts, resulting in the significant augmentation of the mechanical properties. The predictions by the Kozeny-Carman

446 equation verified that the grain surface became rougher due to the calcite precipitation, and
447 showed that the specific surface area likely increased by 1.5 to 3 times as the pore occupation
448 ratio reached 0.10. We have conducted a series of the experiments to understand quantitative
449 evolutions of the physical properties. Although interesting and valuable results were obtained
450 from the experiments, the obtained pore occupation ratio was at most 0.10, and higher ratios
451 should have been attained. As a future study, by improving the grout injection technique, the
452 mechanical and the hydraulic properties at the pore occupation ratios much greater than 0.10 will
453 be investigated quantitatively to unravel the influences of the mineral trapping on those
454 properties.

455

456 **Acknowledgement**

457 This work has been partly supported by research grant from the Research Foundation for the
458 Electrotechnology of Chubu, Nagoya, Japan. Their support is gratefully acknowledged. The
459 authors also thank Mr. Ryota Kashiwagi, Ms. Tomomi Ishimizu and Mr. Hiroki Okahata for their
460 help with the experimental portion of this study.

461

462

463

464

465

6. References

Achal, V., Mukerjee, A., Sudhakara Reddy, M., 2013. Biogenic treatment improves the durability and remediates the cracks of concrete structures. Constr. Build. Mater., 48, 1–5.

Bear, J., 1972. Dynamics of Fluids in Porous Media, Dover Publications, Inc., p. 166.

Bachu, S., Gunter, W. D., Perkins, E. H., 1994. Aquifer disposal of CO2: Hydrodynamic and mineral trapping, Energy Convers. Manag., 35, 269–279.

Czernichowski, I., Sanjuan, B., Rochelle, C., Bateman, K., Pearce, J. M., Blackwell, P., 1996. Analysis of the geochemical aspects of the underground disposal of CO2, in: Apps, J.A., Tsang, C.F. (Eds.), Deep Injection Disposal of Hazardous and Industrial Waste: Scientific and Engineering Aspects. Academic Press, New York, pp. 565–583.

DeJong, J. T., Mortensen, B. M., Martinez, B. C., Nelson, D. C., 2010. Bio-mediated soil improvement. Ecol. Eng., 36, 197–210.

Dvorkin, J., Nur, A., 1996. Elasticity of high-porosity sandstones: Theory for two North Sea data sets, Geophysics, 61, 1363–1370.

Fischer, S., Liebscher, A., De Lucia, M., Hecht, L., & The Ketzin Team., 2013. Reactivity of sandstone and siltstone samples from the Ketzin pilot CO_2 storage site—laboratory experiments and reactive geochemical modeling. Environ. Earth Sci., 70, 3687–3708.

Foppen, J. W. A., Schijven, J. F., 2006. Evaluation of data from the literature on the transport and

484 survival of Escherichia coli and thermotolerant coliforms in aquifers under saturated
485 conditions. Water Res. 40, 401–426.
486 Gunter, W. D., Perkins, E. H., McCann, T. J., 1993. Aquifer disposal of CO2-rich gases: reaction
487 design for added capacity. Energy Convers. Manage. 34, 941–948.
488 Harkes, M. P., van Paassen, L. A., Booster, J. L., Whiffin, V. S., van Loosdrecht, M. C. M., 2010.
489 Fixation and distribution of bacterial activity in sand to induce carbonate precipitation for
490 ground reinforcement. Ecol. Eng., 36, 112–117.
491 Hövelmann, J., Austrheim, H., Jamtveit, B., 2012. Microstructure and porosity evolution during
492 experimental carbonation of a natural peridotite. Chem. Geol. 334, 254–265.
493 Intergovernmental Panel on Climate Change (IPCC), 2005. Special Report on Carbon Dioxide
494 Capture and Storage, in: Metz, B, Davidson, O, de Coninck, H. Loos, M., Meyer, L. (Eds.),
495 Underground geological storage. Cambridge University Press, New York, pp. 195–276.
496 Ivanov, V., Chu, J., 2008. Applications of microorganisms to geotechnical engineering for
497 bioclogging and biocementation of soil in situ. Rev. Environ. Sci. Biotechnol., 7, 139–153.
498 Jaeger, J. C., Cook, N. G. W., Zimmerman, R. W., 2007. Fundamentals of rock mechanics, fourth
499 ed. Blackwell Publishing, Malden, MA.
500 Mitchell, J. K., Santamarina, J. C., 2005. Biological considerations in geotechnical engineering. J.
501 Geotech. Geoenviron. Eng., 131, 1222–1233.

502 Murphy, E. M., Ginn, T. R., 2000. Modeling microbial processes in porous media. Hydrogeol. J.,
503 8, 142–158.
504 Naganume, T., Yukimura, K., Todaka, N., Ajima, S., 2011. Concept and experimental study for a
505 new enhanced mineral trapping system by means of microbially mediated processes, Energy
506 Procedia. 4, 5079–5084.
507 Neupane, D., Yasuhara, H., Kinoshita, N., Unno, T., 2013. Applicability of enzymatic calcium
508 carbonate precipitation as a soil-strengthening technique, ASCE, J. Geotech. Geoenviron.
509 Eng., 139, 2201–2211.
510 Qian, C., Wang, R., Cheng, L., Wang, J., 2010. Theory of microbial carbonate precipitation and its
511 application in restoration of cement-based materials defects. Chin. J. Chem., 28, 847–857.
512 van Paassen, L. A., 2011. Bio-mediated ground improvement: from laboratory experiment to pilot
513 applications. Geo-Frontiers 2011, ASCE, 4099–4108.
514 Whiffin, V. S., van Paassen, L. A., Harkes, M. P., 2007. Microbial carbonate precipitation as a soil
515 improvement technique. Geomicrobiol. J., 24, 417–423.
516 Xu, T., Apps, J. A., Pruess, K., 2003. Reactive geochemical transport simulation to study mineral
517 trapping for CO2 disposal in deep arenaceous formations. J. Geophys. Res. 108(B2), 2071,
518 doi:10.1029/2002JB001979.
519 Yasuhara, H., Neupane, D., Hayashi, K., Okamura, M., 2012. Experiments and predictions of

physical properties of sand cemented by enzymatically-induced carbonate precipitation. Soils Found., 52, 539–549.

Yasuhara, H., Kinoshita, N., Ohfuji, H., Takahashi, M., Ito, K., Kishida, K., 2015a. Long-term observation of permeability in sedimentary rocks under high-temperature and stress conditions and its interpretation mediated by microstructural investigations, Water Resour. Res., 51, doi:10.1002/2014WR016427.

Yasuhara, H., Kashiwagi, R., Kinoshita, N., Lee, D. S., Kishida, K., 2015b. Evaluation of mechanical and hydraulic properties by laboratory experiments simulating mineral trapping of CO_2 sequestration. J. MMIJ, 131, 497–502.